

An optimal discrete-time feedforward compensator for real-time hybrid simulation

Saeid Hayati^a and Wei Song*

Department of Civil, Construction and Environmental Engineering,
The University of Alabama, Tuscaloosa, AL, USA 35487

(Received March 18, 2017, Revised May 27, 2017, Accepted May 29, 2017)

Abstract. Real-Time Hybrid Simulation (RTHS) is a powerful and cost-effective dynamic experimental technique. To implement a stable and accurate RTHS, time delay present in the experiment loop needs to be compensated. This delay is mostly introduced by servo-hydraulic actuator dynamics and can be reduced by applying appropriate compensators. Existing compensators have demonstrated effective performance in achieving good tracking performance. Most of them have been focused on their application in cases where the structure under investigation is subjected to inputs with relatively low frequency bandwidth such as earthquake excitations. To advance RTHS as an attractive technique for other engineering applications with broader excitation frequency, a discrete-time feedforward compensator is developed herein via various optimization techniques to enhance the performance of RTHS. The proposed compensator is unique as a discrete-time, model-based feedforward compensator. The feedforward control is chosen because it can substantially improve the reference tracking performance and speed when the plant dynamics is well-understood and modeled. The discrete-time formulation enables the use of inherently stable digital filters for compensator development, and avoids the error induced by continuous-time to discrete-time conversion during the compensator implementation in digital computer. This paper discusses the technical challenges in designing a discrete-time compensator, and proposes several optimal solutions to resolve these challenges. The effectiveness of compensators obtained via these optimal solutions is demonstrated through both numerical and experimental studies. Then, the proposed compensators have been successfully applied to RTHS tests. By comparing these results to results obtained using several existing feedforward compensators, the proposed compensator demonstrates superior performance in both time delay and Root-Mean-Square (RMS) error.

Keywords: real-time hybrid simulation; feedforward compensator; actuator tracking; servo-hydraulic actuator

1. Introduction

Real-Time Hybrid Simulation (RTHS) is a powerful and cost-effective dynamic experimental technique (Gomez *et al.* 2015). In real-time hybrid simulation (RTHS), the structure under investigation is divided into experimental and numerical substructures. In a typical displacement-controlled RTHS, displacements determined from the numerical substructure of the test are imposed onto the experimental substructures by actuators, and meanwhile, forces generated in the physical components are fed back to the numerical substructure to be used for the displacement calculation of the next time step. This closed-loop process introduces both “time delay” and frequency dependent “time lag” into RTHS (Carrion and Spencer 2007, Carrion *et al.* 2009, Phillips and Spencer 2011).

“Time delay” as it is referred above is not frequency dependent, and sources include communication latency (digital-to-analog and analog-to-digital conversion) and computational time (Carrion and Spencer 2007,

Carrion *et al.* 2009, Phillips and Spencer 2013). On the other hand, the coupled dynamics between the servo-hydraulic actuator and the test specimen introduce “time lag” into RTHS. Time lag depends on both the frequency of excitation and condition of the specimen (Carrion *et al.* 2009, Dyke *et al.* 1995, Phillips and Spencer 2013). A single term—“actuator time delay” or simply “time delay” is used throughout this paper to characterize the overall effect of both time delays and time lags present in the RTHS loop. Actuator time delay generates desynchronization between the numerical and experimental substructures, which causes a destabilizing effect that is equivalent to adding negative damping into RTHS. If this negative damping becomes larger than the inherent damping of the structure, the entire RTHS loop will fail due to instabilities (Darby *et al.* 1999, 2001, Horiuchi *et al.* 1996, Horiuchi *et al.* 1999). Therefore, reducing the actuator time delay is essential to a successful implementation of stable and accurate RTHS. Delay compensation techniques, or simply compensators have been designed to achieve this goal.

Early compensators were designed based on the assumption that actuator time delay is constant. Horiuchi *et al.* (1996), introduced an extrapolation technique in which a polynomial curve is fitted to a certain number of desired displacements obtained previously, and then the future

*Corresponding author, Assistant Professor

E-mail: wsong@eng.ua.edu

^a Ph.D. Candidate

displacement command is predicted by using curve fit. An extrapolation technique was evolved by Darby *et al.* (2001) and Nakashima and Masaoka (1999) where they added interpolation steps into the technique to help the actuator moves smoothly. Later, Chen (2007) and Chen and Ricles (2009a) developed inverse compensation technique based on a simplified actuator delay model. Darby *et al.* (2002) showed that the actuator time delay varies with the stiffness of the experimental substructures during RTHS. Thus, those compensators designed based on a constant delay assumption may have compromised performance when the actual time delay varies during RTHS. Darby *et al.* (2002), Ahmadizadeh *et al.* (2008), Jung and Shing (2006), Chen and Ricles (2009b), and Chae *et al.* (2013) addressed the variation in the actuator time delay in RTHS and developed techniques to update the estimated time delay while the test is in progress. As explained in (Dyke *et al.* 1995), the actuator time delay varies with the condition of the physical test specimen and the excitation frequency. This complicated relationship can be understood by examining the coupled dynamics between an actuator and a specimen, namely control-structure interaction (CSI) (Dyke *et al.* 1995). Therefore, in contrast to the aforementioned compensation techniques that are developed based on delay estimation, model-based compensators are developed based on the dynamic models of the actuator-specimen coupled system to address the specimen and frequency dependency of the time delay. Carrion and Spencer (2007) introduced a model-based feedforward compensator in continuous-time domain based on an experimentally identified dynamic model of the actuator. Later, Phillips and Spencer (2011, 2013) and Phillips *et al.* (2014) integrated a feedback controller into the model-based feedforward compensator to improve its performance. Gao *et al.* (2013) utilized an outer-loop digital H_∞ controller to improve the performance of the hydraulic actuator in RTHS. Ou *et al.* (2015) developed the robust integrated actuator control (RIAC) strategy by integrating a linear-quadratic- estimator and a feedforward controller into the H_∞ strategy.

Table 1 lists the existing RTHS compensators mentioned above which are developed for earthquake engineering research. As shown in this table, most of the compensators have demonstrated effective performance under excitations with a relatively low frequency content (below 15 Hz). This fact has limited the use of RTHS for investigating the dynamic behavior of other engineering systems under relatively higher frequency excitations. For instance, the vibration of a suspension system of a moving vehicle caused by rough road surface can have a frequency bandwidth of 0~20 Hz (Chonhenchob *et al.* 2012, Gillespie and Sayers 1981, Tyan and Tu 2015). The reference tracking performance of the existing compensators mentioned above have not been examined by inputs with such a broad frequency range (0~20 Hz). Thus, herein we propose a discrete-time compensator with only a feedforward structure, which can effectively reduce the actuator time delay when the reference signal has a relatively high frequency bandwidth (e.g., 0~30 Hz).

Table 1 Some of the existing compensators for RTHS

Compensator	Comment	Tracking performance evaluated with frequency range
Extrapolation technique (Horiuchi <i>et al.</i> 1996)	Constant delay	0~10 Hz
Extrapolation with interpolation steps (Darby <i>et al.</i> 2001, Nakashima and Masaoka 1999)	Constant delay	0~10 Hz
Inverse technique (Chen 2007, Chen and Ricles 2009a)	Constant delay	earthquake
Darby <i>et al.</i> (2002)	Varying delay	earthquakes, sinusoidal wave (5 Hz)
Ahmadizadeh <i>et al.</i> (2008)	Varying delay	earthquakes
Feedforward error compensation (Jung and Shing 2006)	Varying delay	earthquakes
Dual compensation (Chen and Ricles 2009b)	Varying delay	earthquake
Adaptive compensation technique (Chen and Ricles 2010)	Adaptive, varying delay	earthquake
Adaptive time series (Chae <i>et al.</i> 2013)	Adaptive, varying delay	earthquake
Model-based feedforward (Carrion and Spencer 2007)	Model-based, feedforward	BLWN* (0~15 Hz)
Model-based feedforward feedback (Phillips and Spencer 2011, 2013, Phillips <i>et al.</i> 2014)	Model-based, feedforward feedback	BLWN* (0~30 Hz)
H_∞ (Gao <i>et al.</i> 2013)	H_∞ controller	earthquake
RIAC (Ou <i>et al.</i> 2015)	H_∞ controller	earthquake

The design of discrete-time model-based compensators has not been fully explored in RTHS. The proposed compensator is designed via different optimization schemes to provide optimal time delay compensation performance. In addition, the proposed compensator adopts a model-based approach to address the specimen and frequency dependency of the time delay. But, unlike the existing mode-based compensators (Carrion and Spencer 2007, Phillips and Spencer 2011, 2013, Phillips *et al.* 2014) that are designed based on the plant model in continuous-time domain, the proposed compensator is developed completely in discrete-time domain. Therefore, we can utilize digital filters with inherently stable formulations in the compensator design, and avoid the frequency warping errors induced by the continuous-time to discrete-time conversion during the compensator implementation in digital computers (Schneider *et al.* 1991). The effectiveness of the proposed compensator is demonstrated through both numerical and experimental studies. Because this study focuses on feedforward compensation, the continuous-time model-based feedforward compensator developed by Carrion and Spencer (2007) and three widely used discrete-

time feedforward compensators developed in other compensation applications (e.g., hard disk drive control) have also been implemented in this study for comparison purposes. They are Non-minimum Phase Zeros Ignore (NPZ-Ignore) Controller (Butterworth *et al.* 2008), Zero Phase Error Tracking Controller (ZPETC) (Tomizuka 1987), and Zero Magnitude Error Tracking Controller (ZMETC) (Wen and Potsaid 2004).

The remainder of this paper is organized as follows. Section 2 of this paper briefly reviews the model-based feedforward compensator in continuous-time domain, NPZ-Ignore, ZPETC, and ZMETC in discrete-time domain. They will be implemented in the study later to compare with the proposed compensator. This section also explains the technical challenge in designing discrete-time compensators which is different than the continuous-time domain development. Section 3 explains and formulates the development of the proposed compensator. Section 4 describes the test bed used for the experimental study and characterizes dynamic models of the plant in continuous-time domain and discrete-time domain. Section 5 investigates the performance of the proposed compensator through the numerical and experimental studies, respectively. This section also investigates the performance of the model-based feedforward compensator, NPZ-Ignore, ZPETC, and ZMETC through experimental studies. The results obtained from RTHS tests by using different compensators are presented in section 6. Section 7 summarizes the paper and provides the conclusions of this study.

2. Existing model-based feedforward compensators

2.1 Feedforward compensators in RTHS

For compensation applications, feedforward control utilizes the knowledge of the input signals and the plant dynamics to control the system outputs to a desirable state. Unlike feedback control, which is only responsive when tracking error starts to develop, feedforward control can directly shape the response to track the command without the knowledge of error, and hence substantially improves the reference tracking performance and speed when the plant dynamics is well-understood and modeled (Marlin 2000). This study focuses on feedforward compensation in RTHS. The essence of feedforward control is to invert the plant dynamics to obtain the corresponding compensator (Goodwin *et al.* 2001). For RTHS, the plant is the dynamic system coupling servo-hydraulic actuator and physical specimen. In some applications, such a feedforward compensator can be non-causal, using previewed information of the input signals (Gross *et al.* 1994). However, due to the looped configuration between numerical and physical components in RTHS, no previewed information of the input signals is available. Therefore, the feedforward compensators used in RTHS are required to be causal and stable. In addition, model-based compensators can consider CSI effects to address the specimen and frequency dependency which is very important for

compensator with a broader applicable frequency range. The rest of this section briefly reviews existing model-based feedforward compensators, including the continuous-time feedforward compensator in (Carrion and Spencer 2007), and three discrete-time feedforward compensators, NPZ-Ignore (Butterworth *et al.* 2008), ZPETC (Tomizuka 1987), ZMETC (Wen and Potsaid 2004). These feedforward compensators are selected as representatives to be compared with the feedforward compensator proposed in this study.

2.2 Continuous-time domain compensators

2.2.1 Model-based feedforward compensator

Carrion and Spencer (2007) proposed a model-based feedforward compensator in continuous-time domain. They showed that the transfer function of the plant (actuator attached to a physical specimen) can be identified using the form below

$$T(s) = \frac{K}{\prod_{i=1}^k (s - p_i)} \quad (1)$$

where $T(s)$ is the transfer function between the desired and measured displacement of the actuator in Laplace transform, s is the variable of Laplace transform, p_i 's are the system poles, $K = \prod_{i=1}^k p_i$ is the gain of the transfer function and k is number of system poles. The direct inverse of Eq. (1) is strictly improper and can result in unbounded responses in RTHS. However, by introducing a unit gain low-pass filter connecting in series with the inverse of the plant model (Eq. (1)), a model-based feedforward compensator with a proper transfer function is obtained. Table 2 shows the transfer function of the model-based feedforward compensator where α is a predefined constant which determines the performance of the compensator. Note that the performance of this compensator improves as α increases, but the value of α should be chosen such that the poles of the compensated plant remain within the Nyquist limit of the digital controller used for RTHS implementations (Carrion and Spencer 2007). Table 2 also formulates the transfer function of the plant after implementing the model-based feedforward compensator.

2.3 Discrete-time domain compensators

The transfer function of the plant in discrete-time domain can be written as

$$T(z^{-1}) = \frac{B^*(z^{-1})}{A^*(z^{-1})} \quad (2)$$

where z is the Z -transform variable and $A^*(z^{-1})$ and $B^*(z^{-1})$ are two reciprocal polynomials which characterize the poles and zeros of the plant, respectively.

In control theory, if the transfer function of a system has all zeros and poles within the unit disk, then the system is called minimum phase (Kailath *et al.* 2000, Oppenheim and Schaffer 2010). The inverse of a minimum phase system is stable, and can be used as a feedforward compensator to remove the dynamic effect of the original system completely. As digital computing and control gain

Table 2 Existing feedforward compensators transfer functions and their corresponding compensated plant transfer functions

Compensator	Time domain	Compensator transfer function	Compensated plant transfer function
Model-based feedforward (Carrion and Spencer 2007)	continuous	$\alpha^k \frac{\prod_{i=1}^k (s - p_i)}{\prod_{i=1}^k (s - \alpha P_i)}$	$\frac{\alpha^k K}{\prod_{i=1}^k (s - \alpha P_i)}$
NPZ-Ignore (Butterworth <i>et al.</i> 2008)	discrete	$\frac{A^*(z^{-1})}{B^{++}(z^{-1}) \cdot B^{--}(1)}$	$\frac{B^{--}(z^{-1})}{B^{--}(1)}$
ZPETC (Tomizuka 1987)	discrete	$\frac{A^*(z^{-1}) \cdot B^-(z^{-1})}{B^{++}(z^{-1}) \cdot B^{--}(1)^2}$	$\frac{B^{--}(z^{-1}) \cdot B^-(z^{-1})}{B^{--}(1)^2}$
ZMETC (Wen and Potsaid 2004)	discrete	$\frac{A^*(z^{-1})}{B^{++}(z^{-1}) \cdot B^-(z^{-1})}$	$\frac{B^{--}(z^{-1})}{B^-(z^{-1})}$

popularities over the years, discrete-time systems arise as sampled continuous-time systems in many engineering fields. However, sampled minimum phase systems are often non-minimum phase (Fu and Dumont 1989, Hagiwara 1996). Åström *et al.* (1984) have shown that a continuous-time system with relative degree larger than two will always generate a discrete-time system with unstable zeros (outside the unit disk) if the sampling frequency is larger than a threshold. Unfortunately, this threshold is reasonably low for many applications and therefore sampled data systems with unstable zeros are quite common. For the plant used in this study, same observation has been made which shows that the zero of the discrete-time transfer function of the plant becomes unstable (therefore non-minimum phase) when the sampling frequency goes beyond 41 Hz. As a result, the inverse of the corresponding discrete-time transfer function will not be stable and cannot be applied directly in RTHS, because the sampling frequency in this study is 1024 Hz, much larger than this threshold. Moreover, sensors and the actuators that are physically non-collocated can cause the system transfer function to be non-minimum phase as well (Butterworth *et al.* 2008). Unlike the issue of improperness in designing continuous-time domain compensators, the inversion of a non-minimum phase system becomes the main technical challenge in designing compensators in discrete-time domain.

In RTHS, the design of compensators based on discrete-time dynamic system model has not been fully explored. But a number of techniques have been developed in other engineering fields to resolve the mentioned stability issue. Three of these techniques are implemented in this research to facilitate the comparison study with the proposed compensator (see Table 2). They are Non-minimum Phase Zeros Ignore (NPZ-Ignore) Controller (Butterworth *et al.* 2008), Zero Phase Error Tracking Controller (ZPETC) (Tomizuka 1987), and Zero Magnitude Error Tracking Controller (ZMETC) (Wen and Potsaid 2004). To explain, the transfer function of a non-minimum phase system is expressed as

$$T(z^{-1}) = \frac{B^*(z^{-1})}{A^*(z^{-1})} = \frac{B^{++}(z^{-1}) \cdot B^{--}(z^{-1})}{A^*(z^{-1})} \quad (3)$$

where the reciprocal polynomials $B^{++}(\cdot)$ and $B^{--}(\cdot)$ contain the stable zeros and unstable zeros of the transfer function, respectively. Because of the unstable zeros in $B^{--}(z^{-1})$, the inverse of the transfer function ($1/T$) is not stable, and cannot be applied directly as a compensator. Several techniques shown below were developed in discrete-time domain to design feedforward compensators for non-minimum phase systems.

2.3.1 Non-minimum Phase Zero Ignore (NPZ-Ignore)

NPZ-Ignore (Butterworth *et al.* 2008) compensator disregards zeros which lie outside of the unit disk and only cancels out the dynamics of the poles and stable zeros of the system. The transfer functions of the NPZ-Ignore compensator and the compensated plant using this compensator are both formulated in Table 2. In these transfer functions, $B^{--}(1)$ guarantees a unit steady-state gain for the compensated plant.

2.3.2 Zero Phase Error Tracing Controller (ZPETC)

ZPETC was introduced by Tomizuka (1987) and designed in a way such that the compensated plant retains the phase of the desired signal (i.e., the Bode phase plot of the compensated plant is equal to zero over the entire frequency range). Although ZPETC has been widely used in many engineering fields, such as motion control and hard disk drive control where previewed information can be obtained for input signal, it cannot be directly applied in RTHS because it is not causal. However, ZPETC can be modified to become causal. Table 2 formulates the ZPETC compensator after modification and the corresponding compensated plant transfer function. In these transfer functions, $B^-(z^{-1}) = z^{-q} \cdot B^{--}(z)$ and q is the degree of the reciprocal polynomial $B^{--}(\cdot)$. Note that the plant after applying the modified ZPETC compensator has a time delay equals q time steps. The modified ZPETC is implemented for the later comparison study in the experimental study section.

2.3.3 Zero Magnitude Error Tracing Controller (ZMETC)

The goal of ZMETC (Wen and Potsaid 2004) is to provide a compensator such that the compensated plant preserves the magnitude of the input signal (i.e., the magnitude of the compensated plant transfer function is

equal to one across the entire frequency range). Again the transfer functions of the ZMETC and the corresponding compensated plant are shown in Table 2.

3. Proposed FIR compensator

As discussed in the introduction, most of the existing compensators used in RTHS have shown successful time delay compensation under inputs with relatively low frequency contents (up to 15 Hz). These compensators are sufficient for use in earthquake engineering research. However, many engineering systems are subjected to relatively higher frequency inputs, such as a vehicle suspension system (Chonhenchob *et al.* 2012, Gillespie and Sayers 1981, Tyan and Tu 2015). To advance RTHS an attractive technique to investigate dynamic behavior of engineering systems working at a relatively high frequency range, this study proposes a novel time delay compensator in discrete-time domain. This compensator aims to provide effective delay compensation performance when subjected to inputs with a higher frequency range (0~30 Hz). In addition, by directly designing the compensator in the discrete-time domain, it enables the use of digital filters with inherently stable formulations, and avoids the frequency warping errors induced by the continuous-time to discrete-time conversion during the compensator's implementation in digital computers (Schneider *et al.* 1991).

3.1 Compensator formulation

In this study, the plant (the servo-hydraulic actuator coupled with the physical specimen) is modeled using an Auto-Regressive with Exogenous (ARX) discrete-time model, which is formulated as

$$y(t) + a_1y(t-1) + \dots + a_{n_a}y(t-n_a) = b_1u(t) + \dots + b_{n_b}u(t-n_b+1) + e(t) \quad (4)$$

where y is the output, which is the measured displacement of the actuator; u is the input which is the desired displacement of the actuator; e is disturbance; n_a equals the number of system poles and n_b equals the number of system zeros plus one. Based on Eq. (4), the corresponding discrete-time transfer function of the plant can be obtained via Z -transform as

$$T(z^{-1}) = \frac{b_1 + \dots + b_{n_b}z^{-n_b+1}}{1 + a_1z^{-1} + \dots + a_{n_a}z^{-n_a}} \quad (5)$$

As explained in section 2, the above transfer function is likely to be non-minimum phase and can be rewritten in the same form as Eq. (3), based on the characteristics of its zeros. Instead of directly inverting the transfer function $T(z^{-1})$, which will result in an unstable system, this study proposes the compensator G_{FIR} to take the following form

$$G_{FIR}(z^{-1}) = \frac{A^*(z^{-1})}{B^{**}(z^{-1})} \cdot H(z^{-1}) \quad (6)$$

where $H(z^{-1})$ is the term to approximate the inverse of $B^{**}(z^{-1})$, and is defined as a finite impulse response (FIR)

filter

$$H(z^{-1}) = h_1 + h_2z^{-1} + \dots + h_nz^{-n+1} \quad (7)$$

Here, h_1, h_2, \dots, h_n are n unknown parameters of the compensator, which will be determined by an optimization process explained in section 3.2. One of the properties of FIR that has been exploited here is that FIR filter is inherently stable. Because of the use of FIR, G_{FIR} is used to denote the proposed compensator in Eq. (6), and it is termed as "FIR compensator" in this paper. The compensated plant using the FIR compensator is expressed as

$$T_{com}(z^{-1}) = T \cdot G_{FIR} = B^{**}(z^{-1}) \cdot H(z^{-1}) \quad (8)$$

In which T and G_{FIR} are formulated in Eqs. (3) and (6).

3.2 Optimization schemes

The goal of this study is to determine $H(z^{-1})$, such that the resulting compensator G_{FIR} can provide effective time delay compensation performance up to a specific cut off frequency, f_c . Fig. 1 shows a schematic Bode plot of the compensated plant transfer function T_{com} (Eq. (8)).

In Fig. 1, the frequency range from 0 to f_c is called passband and the frequency range from f_c to Nyquist frequency is called stopband. Ideal compensation performance demands the magnitude of T_{com} be equal to one and the phase of T_{com} be equal to zero within the passband. To achieve this goal, three different optimization schemes, *Least Square* (LS), *Weighted Least-Square* (WLS), and *MiniMax* (MM) are defined and are applied to determine $H(z^{-1})$, Eq. (7), in FIR compensator. To formulate the optimization problem, the frequency domain is discretized by N discrete points, f_i 's with $i = 1, \dots, N$ (see Fig. 1). Before introducing the objective functions, note that the Z -transform variable, z , is related to the frequency as

$$z = e^{j\omega\delta t} = e^{j2\pi f\delta t} \quad (9)$$

where δt is the sampling period; ω denotes circular frequency; f denotes frequency and j is the imaginary unit ($\sqrt{-1}$) which retains its definition throughout the whole paper. With Eq. (9), the transfer function $T_{com}(z^{-1})$ (Eq. (8)) in z -domain is mapped into $T_{com}(f_i)$ in frequency domain for Bode plot (frequency response) calculation. The objective function of WLS scheme is defined as

$$\min_{h_1, h_2, \dots, h_n} \left\{ \sum_i w_i \cdot \|T_{com}(f_i; h_1, h_2, \dots, h_n) - 1\|^2 \right\}, \quad (10)$$

$$\begin{cases} w_i \geq 1 & \text{for } f_i \in \text{passband} \\ w_i = 1 & \text{for } f_i \in \text{stopband} \end{cases}$$

In Eq. (10), h_1, h_2, \dots, h_n are n compensator parameters to be determined for $H(z^{-1})$ (Eq. (7)); f_i denotes the i^{th} discretized frequency point; w_i is the weight associated with the i^{th} discretized frequency; $T_{com}(f_i)$ is the complex value of the compensated plant

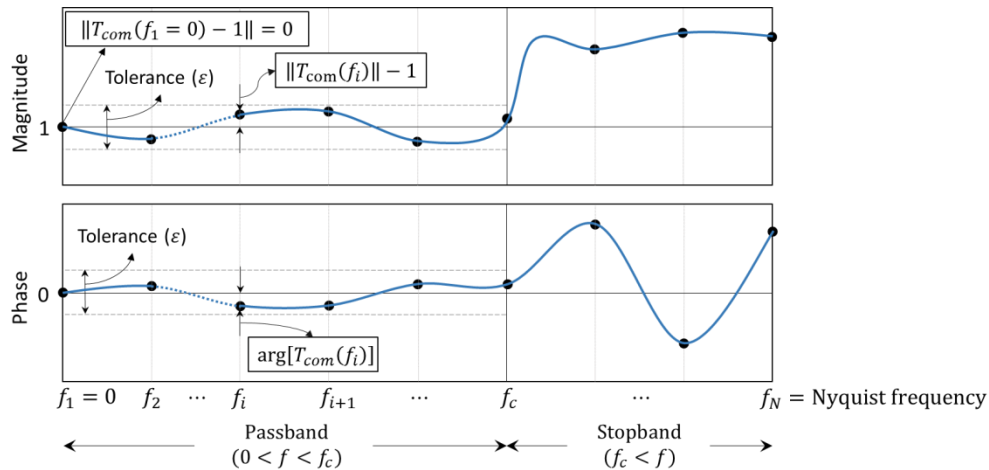


Fig. 1 Schematic Bode plot of compensated plant transfer function

transfer function (Eq. (8)) at frequency f_i ; and $\|\cdot\|$ indicates the modulus of complex number which in this paper is the norm of error between the compensated plant transfer function and one. A larger w_i means a higher importance is placed on the error norm at frequency f_i . In this study, the objective function of WLS scheme has $w_i = 1000$ for points in the passband and $w_i = 1$ for points in the stopband.

The same objective function as shown in Eq. (10) is used for LS scheme with $w_i = 1$ for points in both the passband and stopband. On the other hand, MM objective function minimizes the maximum of the absolute of the compensated plant transfer function. The objective function for MM is formulated in Eq. (11).

$$\min_{h_1, h_2, \dots, h_n} \{ \max_{f_i \in \text{stopband}} \|T_{\text{com}}(f_i; h_1, h_2, \dots, h_n)\| \}, \quad (11)$$

The same constraints are applied to all three optimization schemes

- Steady-state gain is equal to one (see Fig. 1), i.e.

$$\|T_{\text{com}}(f = 0; h_1, h_2, \dots, h_n) - 1\| = 0 \quad (12)$$

- Magnitude of the compensated plant across the passband is equal to one (see Fig. 1), i.e.

$$\sqrt{\sum_{f_i \in \text{passband}} (\|T_{\text{com}}(f_i; h_1, h_2, \dots, h_n)\| - 1)^2} = 0 \quad (13)$$

- Phase of the compensated plant across the passband is equal to zero (see Fig. 1), i.e.

$$\sqrt{\sum_{f_i \in \text{passband}} \{ \arg[T_{\text{com}}(f_i; h_1, h_2, \dots, h_n)] \}^2} = 0 \quad (14)$$

where $\arg(\cdot)$ determines the argument of a complex number. In the implementation of these constraints, a

tolerance ϵ is applied on the right-hand-side of Eqs. (12)-(14) instead of zero to improve the convergence of the optimization process. Fig. 1 also schematically demonstrates the use of tolerance ϵ . Choosing different number of parameters (n) for $H(z^{-1})$, different values for cut off frequency (f_c), and different optimization schemes will lead to different FIR compensators with different performances. Detailed comparison will be demonstrated in the following numerical and experimental studies. MATLAB (MATLAB 2014) Optimization Toolbox was used to solve the optimization problem formulated above.

4. Test-bed and characterization of plant model

To demonstrate the effectiveness of the proposed compensator, a test-bed for this study is set up by attaching a linear spring-mass system to a servo-hydraulic actuator (See Fig. 2). Such a linear test-bed aims to provide a fair environment with constant specimen condition for the later comparison study of different compensators. The load capacity of the actuator is 110 kips (489 kN) with a stroke of ± 10 inches (± 0.254 m). The mass box weighs 1278 lb (580 kg), and the stiffness of the spring is 8 kips/in (1403 kN/m). The sampling frequency of the digital controller is 1024 Hz. All the experiments were carried out in the Large Scale Structures Laboratory (LSSL) at The University of Alabama.

To characterize the plant for design of the compensators, 10 BLWNs with different bandwidth frequencies ($= 0\text{--}64, 0\text{--}128$ Hz) and different maximum amplitudes ($= 0.1, 0.2, 0.5, 1, \text{ and } 1.5$ in, corresponding to 2.54, 5.08, 12.7, 25.4, and 38.1 mm) were used as the desired signal. Based on the acquired data, two different dynamic models according to the time domain were generated for the actuator, one for a continuous-time compensator and the other for a discrete-time compensator design.



Fig. 2 Experimental setup in the LSSL at The University of Alabama

Table 3 Poles of two fitted transfer functions for the plant

	No. poles (k)	p_1	p_2	p_3	p_4	K
Model #1	3 poles	-128.06	$-32.08 + 87.34j$	$-32.08 - 87.34j$	Not applicable	1.155×10^6
Model #2	4 poles	$-119.39 + 186.34j$	$-119.39 - 186.34j$	$-37.77 + 78.93j$	$-37.77 - 78.93j$	3.834×10^8

4.1 Continuous-time plant model

Desired signals, together with the corresponding measured displacements of the actuator, were used as system input and output, respectively, to generate the transfer function of the plant. All the 10 sets of recorded data under various input signals have led to similar frequency responses for the plant. Two transfer function models based on Eq. (1) were fitted using the frequency response obtained from the experiments, one using a 3-pole formulation and one using a 4-pole formulation. The obtained poles and gains of these two models are shown in Table 3.

Then, by using these two fitted transfer functions and different values of $\alpha = 3, 5, 7$, and 10, eight model-based feedforward compensators (see Table 2) were designed for later comparison study.

4.2 Discrete-time plant model

Discrete-time transfer function was also obtained by using the same recorded data. A total of 841 ARX models (Eq. (4)) with different number of n_a and n_b were obtained. Another 72 new data sets (different than the data sets used to obtain the transfer function) were used to verify the obtained models. During the model verification process, Bayesian Information Criterion (BIC) formulated below has been considered to select the best fitted model corresponding to the collected data (72 data sets)

$$\text{BIC} = \ln(\text{MSE}) + \ln(N) \times \frac{\text{dim}}{N}; \quad (15)$$

$$\text{MSE} = \frac{\sum_{i=1}^N [e(t_i)]^2}{N}$$

In Eq. (15), N is the total number of samples, $\text{dim} = n_a + n_b$ is the total number of parameters in the fitted ARX model and MSE is the Mean Square Error which is also formulated in Eq. (15). In MSE, $e(t_i)$ is the error between the fitted model and the captured data at step i .

The model that generates the smallest value based on Eq. (15) is considered as the “best” fitted model. This process performed for all 72 data sets generated for the model

verification. A histogram plot was made to see how frequently a model is selected as the best model. The model with the highest occurrence in the histogram plot was considered as the best ARX model of the plant based on BIC criterion. Using this best fitted ARX model, a discrete-time domain transfer function can be obtained in the form of Eq. (3). The numerator and denominator terms of this transfer function are presented in Eq. (16)

$$\begin{aligned} B^{*+}(z^{-1}) &= 1 \\ B^{-*}(z^{-1}) &= -5.508 \times 10^{-5} + 9.164 \times 10^{-5} z^{-1} \\ A^*(z^{-1}) &= \text{An 8}^{\text{th}} \text{ degree polynomial} \end{aligned} \quad (16)$$

According to Eq. (16), the transfer function of the plant has one unstable zero ($z = 1.664$) which can be calculated by letting $B^{-*}(z^{-1}) = 0$. This unstable zero causes the plant to be non-minimum phase. The denominator of the plant transfer function ($A^*(z^{-1})$) has a degree of 8 and for clarity, this term is not shown in Eq. (16). This transfer function was used for designing NPZ-Ignore, ZPETC, ZMETC compensators, and the proposed FIR compensator. All the model fitting procedures described in this section are coded in MATLAB (MATLAB 2014), for both continuous-time plant models and discrete-time plant models.

5. Compensation performance study

To demonstrate the efficacy of the proposed discrete-time compensator, both numerical and experimental studies are conducted to examine the compensation performance of the proposed compensator. Through these studies, the performance of the proposed compensators are compared with four existing feedforward compensators: model-based feedforward compensator (Carrion and Spencer 2007) in continuous-time domain, NPZ-Ignore (Butterworth *et al.* 2008), ZPETC (Tomizuka 1987), and ZMETC (Wen and Potsaid 2004) compensators in discrete-time domain. Three different BLWNs with bandwidth = 0~10, 0~20, and 0~30 Hz and maximum amplitude of 0.2 in (0.00508 m) are used for studying the performance of the compensators. Different bandwidths of white noises are representing different frequency content level of the desired signals: low (0~10 Hz), medium (0~20 Hz) and high (0~30 Hz) levels.

5.1 Compensation performance indicators

In this paper, the compensation performance is evaluated based on two metrics: time delay and relative Root-Mean-Square (RMS) error.

5.1.1 Time delay

The time delay in the RTHS can be characterized by the slope of the secant line in the Bode phase plot at a given frequency. It can be calculated as below (Oppenheim and Schaffer 2010, Smith 2008)

$$\text{Time delay } (\omega) = -\frac{\arg[T(\omega)]}{\omega} \quad (17)$$

where $\arg(\cdot)$ is the argument of a complex number in radian and ω is the given circular frequency where the time delay is calculated. In this study, the delay indicator is determined as the averaged time delay calculated using Eq. (17) within the frequency range of the input signal. Because the sampling frequency of the test-bed is 1024 Hz, which corresponds to a 0.97 millisecond (ms) sampling period, the goal of the delay compensation is to reduce the overall time delay to less than 1 ms (i.e., less than 1 time step). In that case, the desired displacement and the measured displacement of the actuator can be effectively considered as “synchronized”. Note that a lower value for time delay indicates a better compensation performance.

5.1.2 Relative Root-Mean-Square (RMS) error

The relative RMS error between the desired displacement and the measured displacement of the actuator is another compensation performance indicator. It is defined as

$$\text{RMSE}_{\text{CMP}}(\%) = \frac{\sqrt{\sum_i (d_i^m - d_i^d)^2}}{\sqrt{\sum_i (d_i^d)^2}} \times 100 \quad (18)$$

where d_i^m and d_i^d are the actuator measured displacement and the desired displacement at time step i , respectively. Note that a lower value for the relative RMS error indicator corresponds to a better compensation performance.

5.2 Numerical study

Based on the obtained discrete-time transfer function formulated in Eqs. (3) and (16), a total of 72 FIR compensators (Eq. (6)) were designed by using the 3 different optimization schemes (WLS, LS and MM), with 6 predetermined different numbers of parameters ($n = 25, 50, 75, 100, 200$ and 300), and 4 different cut off frequencies settings ($f_c = 32, 64, 96$ and 128 Hz). Note that choosing a large value for the number of parameters increases the computational demand which can potentially fail the real-time requirement in RTHS. As a result, the number of parameters considered is limited to less than 300 in this study. Before investigating the performance of these newly designed FIR compensators in the laboratory, numerical simulations were conducted to examine their behaviors using the two performance indicators established in section 5.1.

5.2.1 Numerical performance study of FIR compensator under the BLWN with bandwidth = 0~20 Hz

In this section, time delay and relative RMS error indicators are used to investigate the performance of the FIR compensators under the BLWN with bandwidth = 0~20 Hz and maximum amplitude = 0.2 in (0.00508 m) through numerical study.

Time delay

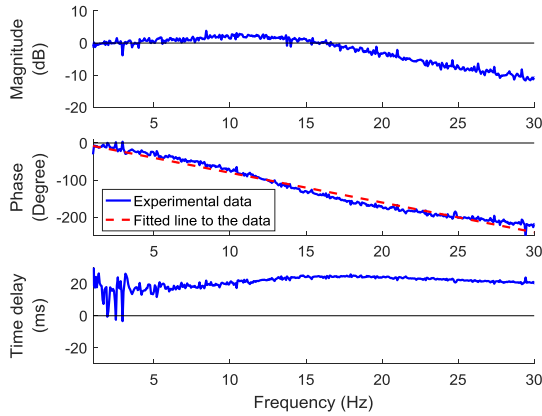
Plot (a) of Fig. 4, shows the time delay of the compensated plant (Eq. (8)) after applying FIR compensators obtained based on WLS optimization scheme. Black points on the surface are associated with 24 out of 72 FIR compensators designed by using different number of parameters and different values for cut off frequency. Fig. 5 follows the same convention as well. The surface in plot (a) of Fig. 4 is generated by interpolating among the time delays calculated based on Eq. (17) for each of these 24 FIR compensators to capture the trend of the delay. The plot indicates that all FIR compensators successfully reduced the actuator time delay to less than 1 ms which is the goal of delay compensation. Another observation is that the time delay associated with the FIR compensator decreases as the number of parameters (n) increases. Also choosing a smaller value for cut off frequency (f_c) leads to a compensator which reduces the time delay further, but of course with a smaller compensation range. Similar time delay surfaces have been seen for the rest of 48 FIR compensators obtained based on LS and MM optimization schemes and therefore those results are not shown here for brevity.

Relative RMS error

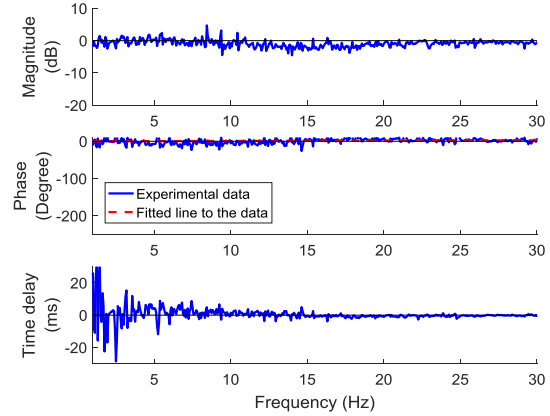
Plot (a) of Fig. 5 presents the relative RMS error between the desired displacement and measured displacement of the actuator after applying FIR compensator obtained based on LS optimization scheme. The surface in this plot is generated by interpolating among the relative RMS error calculated based on Eq. (18) for each of the 24 FIR compensators obtained by using different number of parameters and different values for cut off frequency. Similar to the time delay (see Fig. 4, plots (a)), the relative RMS error decreases as the number of parameters increases and cut off frequency decreases. Another observation based on plots (a) is that the relative RMS errors corresponding to compensators with $f_c = 32$ Hz do not follow the dominant trend. This difference may be due to the fact that the frequency content of the desired signal (0~20 Hz) is relatively close to the cut off frequency of the compensator (32 Hz), and therefore the compensation performance is limited. This observation implies that the selected cut off frequency (f_c) for the compensator should be relatively large compared to the frequency content of the input signal to achieve a good RMS compensation performance. Similar relative RMS error performance trends for the rest of 48 FIR compensators obtained based on WLS and MM have been observed and for succinctness are not shown in Fig. 5.

Table 4 Time delay and relative RMS error of the actuator without compensation

Actuator time delay based on different methods (ms)			
Input bandwidth (Hz)	Average of the slope of the secant lines in the Bode phase plot (Eq. (17))	Slope of the fitted line to the Bode phase plot (see Fig. 3)	Relative RMS error (%)
0 ~ 10	16.7	17.8	75.6
0 ~ 20	20.8	23.4	135.2
0 ~ 30	21.1	22.3	137.3



(a) Before compensation



(b) After compensation

Fig. 3 Bode plot of the plant and the corresponding time delay (Input displacement: BLWN with bandwidth = 0~30 Hz and max. disp. = 0.2 in (0.00508 m)): (a) Results before applying any compensators and (b) Results after applying FIR compensator obtained from LS schemes with $n = 200$ and $f_c = 64$ Hz

5.3 Experimental study

The experimental study was conducted in LSSL using the setup shown in Fig. 2. The compensation performance of the total 72 FIR compensators and 4 existing feedforward compensators were investigated. The input signals are three BLWNs with bandwidth of 0~10, 0~20, and 0~30 Hz and a maximum amplitude = 0.2 in (0.00508 m).

Time delay and relative RMS error when the actuator is subjected to the 3 mentioned BLWNs without any compensation are presented in Table 4. The time delays reported in the second column are calculated using the method described in section 5.1.1. The third column of Table 4 reports the slope of a fitted straight line to the Bode phase plot of the plant which can also represent the time delay. Slightly different delay estimations (under 3 ms) are obtained with these two different methods. Again, the averaged delay calculated using Eq. (17)—second column in Table 4, is used as the time delay indicator in this paper.

The Bode plot of the plant without any compensation is shown in Fig. 3(a). In the same figure, the actuator time delay calculated by using Eq. (17) is presented underneath the Bode plot. Here, the frequency dependency of the time delay is clearly demonstrated by the varying slope of the phase plot. The averaged time delay is 21.1 ms. In the Bode phase plot of Fig. 3(a), a fitted straight line passing through

the origin serves as a graphical indicator for the time delay. The slope of this fitted line is also presented as the time delay in Table 4. Actuator time delay shown in Fig. 3(a) can be reduced effectively by implementing the proposed FIR compensators. Fig. 3(b) illustrates the Bode plot of the plant after implementing the FIR compensator generated by LS scheme with $n = 200$ and $f_c = 64$ Hz. The average of time delay calculated based on phase angle (Eq. (17)) is 0.342 ms, which is a significant improvement comparing to the time delay before compensation, 21.1 ms (see Table 4).

As mentioned above, three sets of BLWNs with bandwidth 0~10 Hz, 0~20 Hz and 0~30 Hz have been used as input signals to examine the performance of the proposed FIR compensator. Under the BLWN of lower frequency bandwidth 0~10 Hz, the proposed FIR compensator successfully reduced the time delay from 16.7 ms (see Table 4) to less than 1 ms, and the relative RMS error was reduced from 75.6% (see Table 4) to less than 7%. In addition, the performance trend of the FIR compensator under the bandwidth = 0~10 Hz is similar to the performance trend under bandwidth = 0~20 Hz and 0~30 Hz. Therefore, this paper focuses on presenting only the performance of the FIR compensator under the more challenging cases using BLWNs with medium (0~20 Hz) and high (0~30 Hz) bandwidth. The performance of the proposed compensator under the BLWN with bandwidth = 0~20 Hz is shown in section 5.3.1. And the performances of

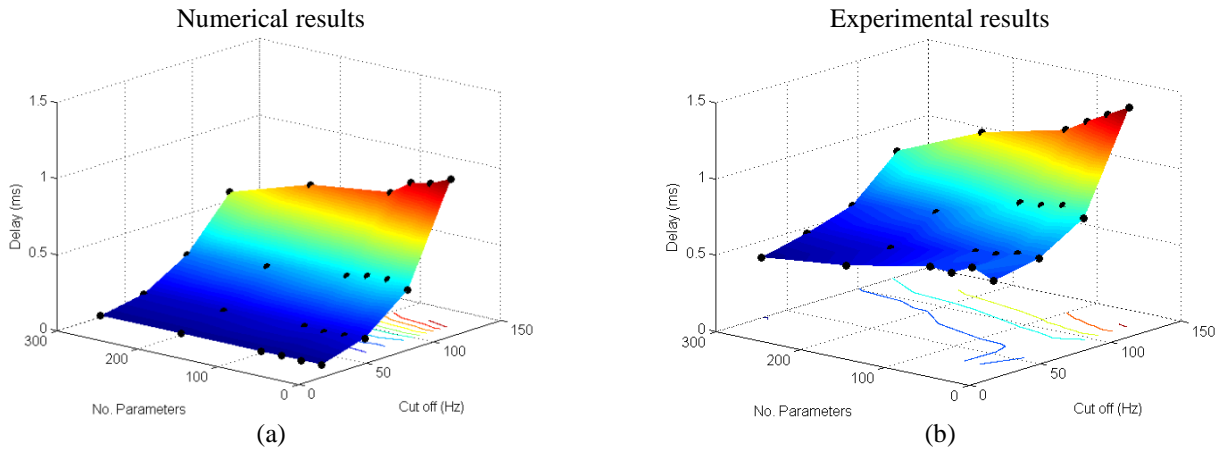


Fig. 4 Time delay after applying FIR compensators obtained based on WLS optimization scheme. (a): Numerical study and (b): Experimental study. (Input: BLWN with bandwidth = 0~20 Hz and maximum amplitude = 0.2 in (0.00508 m))

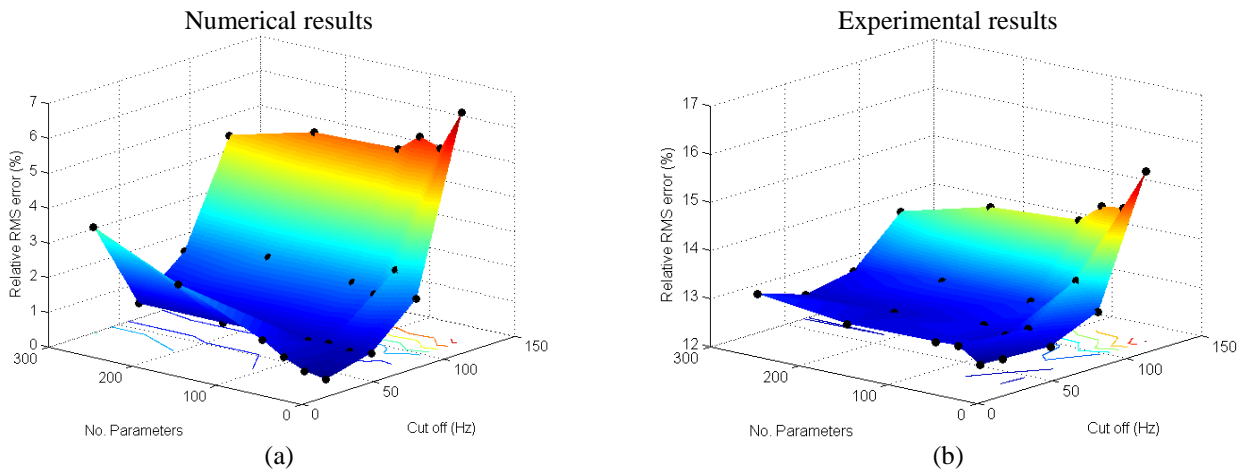


Fig. 5 Relative RMS error between the desired and the measured displacement of the actuator after applying FIR compensators obtained based on LS optimization scheme. (a): Numerical study and (b): Experimental study. (Input: BLWN with bandwidth = 0~20 Hz and maximum amplitude = 0.2 in (0.00508 m)).

FIR compensator, model-based feedforward compensator, NPZ-Ignore, ZPETC, and ZMETC under the BLWN with bandwidth = 0~30 Hz are shown in section 5.3.2.

5.3.1 Experimental performance study of FIR compensator under BLWN with bandwidth = 0~20 Hz

Time delay

Plot (b) in Fig. 4 summarizes the averaged time delay of 24 FIR compensators via experimental tests under the BLWN signal with bandwidth = 0~20 Hz and maximum amplitude = 0.2 in (0.00508 m). All these 24 FIR compensators were obtained using WLS optimization scheme. As it can be seen from this plot, most of the FIR compensators have effectively reduced the time delay to less than 1 ms. Note that the time delay before applying the compensator was 20.8 ms (see Table 4). According to these experimental results, the same trend for the time delay associated with the FIR compensator, as was seen in the numerical study (plots (a) in Fig. 4) can also be observed for the experimental results, i.e., a larger value for the

number of parameters leads to a smaller time delay, and a larger value of cut off frequency results in a larger time delay. As a result, the FIR compensator with a smaller cut off frequency, such as 32 Hz, and a larger number of parameters, such as 300, can reduce the time delay to less than a half of millisecond. Similar time delay surfaces have been observed for the rest of 48 FIR compensators obtained using LS and MM optimization schemes, and therefore the results are not shown here for brevity.

Relative RMS error

The relative RMS error of the 24 FIR compensators under the BLWN signal with bandwidth = 0~20 Hz are shown in plot (b) of Fig. 5. All these 24 FIR compensators were obtained using LS optimization scheme. The relative RMS error with no compensation is 135.2% (see Table 4).

As it can be observed, all the FIR compensators reduced the relative RMS error to less than 16%.

Similar performance trend, as was observed in the numerical study (plots (a) of Fig. 5), can also be seen for the experimental results, i.e., a larger value for the number of

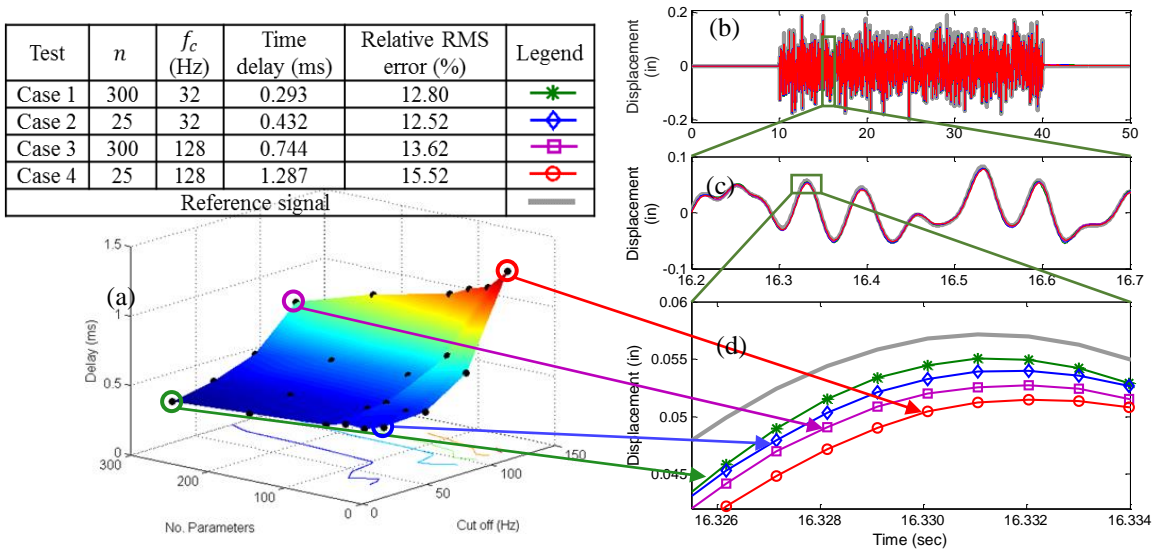


Fig. 6 Experimental results for LS scheme. (a): Delay plot for system with different LS compensators, (b): Time history displacement response of the plant to BLWN with bandwidth = 0~20 Hz and maximum amplitude = 0.2 in (0.00508 m); (c) and (d): Zoom-in view of the plant response

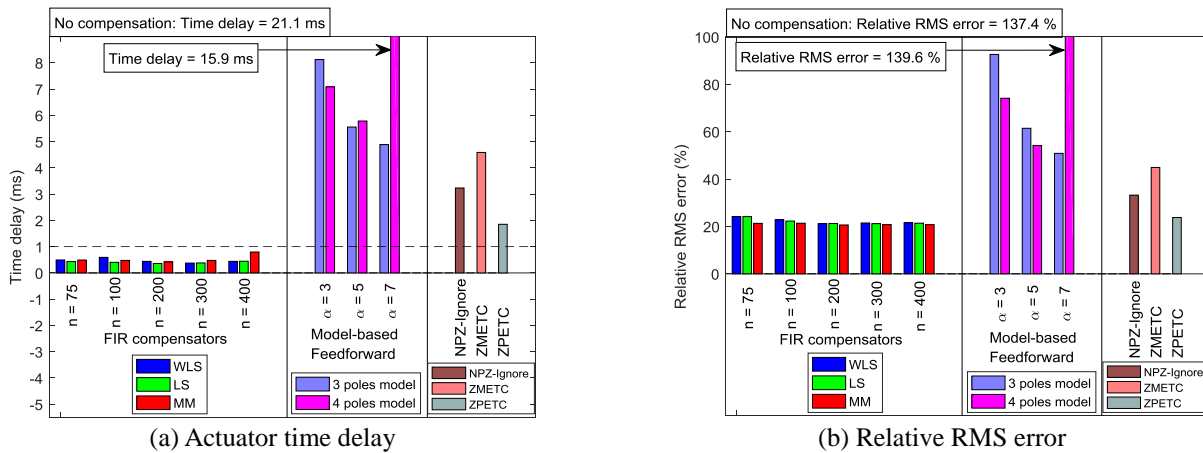


Fig. 7 Actuator time delay and relative RMS error obtained from experimental study. Input: BLWN with bandwidth = 0~30 Hz and maximum amplitude = 0.2 in (0.00508 m)

parameters leads to a smaller relative RMS error, and a larger value of cut off frequency results in a larger relative RMS error. Similar relative RMS error performance trends for the rest of 48 FIR compensators obtained based on WLS and MM optimization schemes were seen and for brevity are not shown in Fig. 5.

An interesting observation made between the numerical results and the experimental results (Figs. 4 and 5) is that, although the general trends revealed in the surface plots are very similar, the estimated time delay and relative RMS error obtained in the experimental studies are elevated comparing to the corresponding numerical results. It may be due to the uncertainties or modeling error in characterizing the plant model, which in turn affects the performance of the derived feedforward compensator.

Time history responses

Time history responses of the actuator for 4 different FIR compensators (LS optimization scheme with $n = 25$ and 300 and $f_c = 32$ and 128 Hz) are presented in Fig. 6. As shown in Fig. 6(a), the four selected cases represents the data points located at the four corners of the surface obtained in Fig. 4(e). Plots (b) of this figure shows the time history of the desired and measured displacements of the actuator. The desired displacement for these tests was the BLWN with bandwidth = 0~20 Hz and maximum amplitude = 0.2 in (0.00508 m). In plots (c) and (d) of Fig. 6, the zoom-in views of the displacement time histories illustrate that even though all the four FIR compensators provide good compensation performance for the actuator, the best performance is achieved by the FIR compensator with $n = 300$ and $f_c = 32$ Hz, and the least effective performance out of the four is achieved by the FIR compensator with $n = 25$ and $f_c = 128$ Hz.

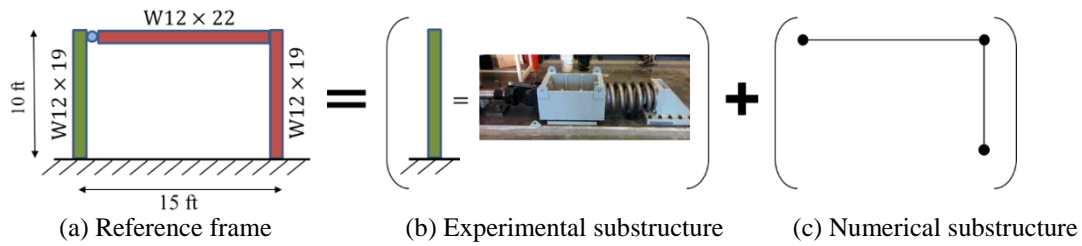


Fig. 8 RTHS setup

This observation in time domain matches with the observation seen in the time delay surface. The averaged time delay and the relative RMS error for these four cases are recorded in the table inserted inside of Fig. 6. As it can be seen, the relative RMS error for these four FIR compensators follows the same trend as the time delay.

5.3.2 Experimental performance study of all compensators under BLWN with bandwidth = 0~30 Hz

The performance of the proposed compensator under the BLWN with bandwidth = 0~30 Hz and maximum amplitude = 0.2 in (0.00508 m) was also studied experimentally. For this set of tests, 15 FIR compensators with $f_c = 64$ Hz and $n = 75, 100, 200, 300,$ and 400 were considered.

To compare, the performance of six model-based feedforward compensators (designed based on two obtained continuous-time plant models (see Table 3) and $\alpha = 3, 5,$ and 7), NPZ-Ignore, ZPETC and ZMETC compensators were also implemented and studied. Note that this paper is introducing a feedforward compensator (i.e., no measured feedback signal is used), and as a result, the performance of this compensator was only compared with those aforementioned feedforward compensators. Again, two indicators, time delay and relative RMS error, were used to investigate the compensation performance.

Time delay

Fig. 7(a), shows the average of the actuator time delay determined based on Eq. (17) for all compensators. The actuator time delay without any compensation was 21.1 ms (see Table 4). All the considered feedforward compensators have demonstrated successful compensation performance. However, the FIR compensators are the only ones that reduced the time delay to less than 1 ms which is the goal of compensation. Fig. 7(a) shows that the time delay associated with the model-based feedforward compensator decreases as the value of α increases. For $\alpha = 7$, the compensator designed based on model #2 (see Tables 3 and 4 poles model) is no longer effective.

Relative RMS error

Fig. 7(b) illustrates the relative RMS error calculated based on Eq. (18) for all compensators. The relative RMS error under the BLWN with bandwidth = 0~30 Hz with no compensation was 137.4% which was reduced after utilizing the feedforward compensators. Similar to the time delay compensation performance, the best relative RMS errors were observed to be associated with the FIR

compensators. Also, it can be seen that the ZPETC compensator reduced the relative RMS error very well.

6. Real-time hybrid simulation

The performance of the proposed compensator is also investigated under RTHS, and the results were compared with some of the existing feedforward compensators.

6.1 Reference structure

A one bay-one story steel frame as shown in Fig. 8 is considered as the reference structure. The cross sections for the two columns are 10 feet long $W12 \times 19$, and 15 feet long $W12 \times 22$ for the beam. A concrete slab on top of the frame serves as the floor to the frame and adds a uniform distributed mass to the frame. Rayleigh damping for the entire model is assumed such that the first and second mode of the frame have 5% damping ratio. The first two natural frequencies of the frame are 0.480 and 5.64 Hz, respectively. The upper left joint of the frame is a pinned connection, while the upper right joint is a moment resistant connection, and both of the supports of the frame are fully fixed to the ground. The input to this reference frame is ground motion. For RTHS, the frame is divided into two parts: the left column is the experimental substructure, which is represented by the test-bed described in Fig. 2, and the rest of the frame is the numerical substructure modeled using Euler beam element (see Fig. 8(c)). The length and the steel cross section $W12 \times 19$ are chosen for the column, such that the natural frequency of the spring-mass system in the test-bed (see Fig. 2) is the same as the natural frequency of the first lateral mode of the left column. The rest of the frame, including the floor mass, represents the numerical substructure (Fig. 8(c)) and is simulated in Simulink Real-Time[®] (MATLAB 2014). Moreover, a mathematical model of the entire reference frame is simulated in MATLAB to capture the response of the entire frame subjected to ground motion.

For the performance evaluation purpose, besides the time delay and the relative RMS error between the actuator input and output signals, the comparison between the simulated response of the entire frame and the response obtained from RTHS also provides a valid indicator of the performance of the compensators. It is defined as

$$RMSE_{RTHS}(\%) = \frac{\sqrt{\sum_i (d_i^m - d_i^s)^2}}{\sqrt{\sum_i (d_i^s)^2}} \times 100 \quad (19)$$

where d_i^s and d_i^m are the simulated displacement and the measured displacement during RTHS at time step i , respectively. In this study, the displacement of interest is the lateral degree-of-freedom (DOF) of the top of the left column, which is the interfacing DOF between the numerical and experimental substructures.

6.2 Real-time hybrid simulation test

Two different ground acceleration records were imposed to the frame to perform the RTHS: 1) El Centro record and 2) BLWN with bandwidth = 0~20 Hz. To avoid damaging the experimental set up during the test, the maximum acceleration of El Centro record and BLWN were set to be 0.033 g and 0.013 g, respectively. The FIR compensators obtained using the three different optimization schemes (WLS, LS, and MM) with $f_c = 32$ Hz and $n = 75, 100, 200, 300$ and 400 are chosen for the RTHS study, because of the good performance they have demonstrated during the experimental studies (Figs. 4, 5 and 7). In addition, 6 model-based feedforward compensators (designed based on two different dynamic models of the actuator (Table 3) with $\alpha = 5, 7$, and 10), NPZ-Ignore, ZMETC and ZPETC compensators were also implemented for RTHS to provide comparison results.

6.2.1 Time history responses

Fig. 9 depicts the results of RTHS tests carried out with 3 different FIR compensators ($n = 300$, $f_c = 32$ Hz, and 3 different optimization schemes) and the simulated response of the entire frame when it is excited by El Centro acceleration record. For clarity, the results of RTHS without delay compensation is not presented in this figure. Figs. 9(a) and 9(b) show time histories of the measured restoring force and the measured displacement of the actuator (i.e., responses of the frame at interfacing DOF), respectively. Based on these two plots, a good agreement between the results obtained from RTHS tests and the simulated responses of the entire frame can be observed. A zoom-in view of displacement time history response is shown in Fig. 9(c). This plot shows that all RTHS tests carried out by using these three FIR compensators were successful. The performance of these three FIR compensators together with 12 other FIR compensators, model-based feedforward, NPZ-Ignore, ZPETC and ZMETC compensators are shown later on in this paper. Fig. 9(d) shows the measured restoring force versus the measured displacement of the actuator. The observed straight line in this plot indicates a linear relationship between the force and displacement responses of the experimental substructure which verifies that it is indeed a linear spring-mass system (see Fig. 2). The slope of this line (8 kips/in) is equal to the stiffness of the spring which has the same value as measured from a set of static experiments. These observations demonstrate that FIR compensators effectively improved the performance of the actuator and led to successful RTHS tests.

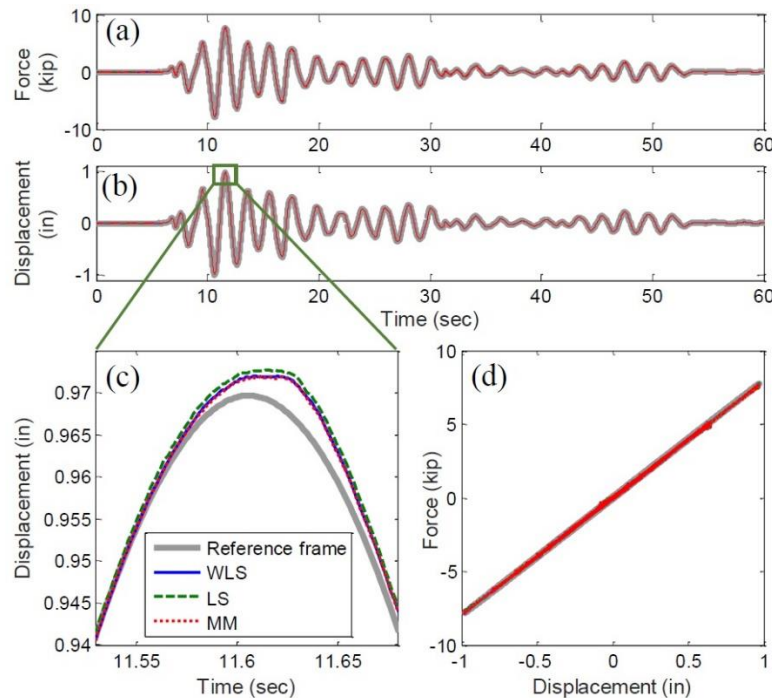


Fig. 9 Time history responses of the frame at the interfacing DOF to the El Centro excitation. (a): Time history of the measured restoring force of the actuator, (b): Time history of the measured displacement of the actuator, (c): Zoom-in view of the time history of the measured displacement of the actuator and (d): Restoring force versus displacement. Note: all three FIR compensators have $n = 300$ and $f_c = 32$ Hz

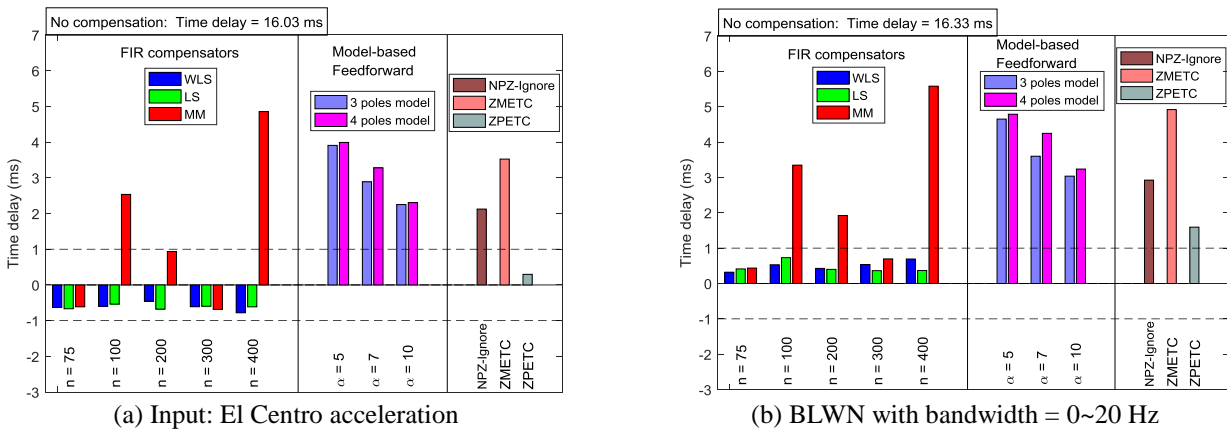


Fig. 10 Actuator time delay after implementing different compensators in RTHS

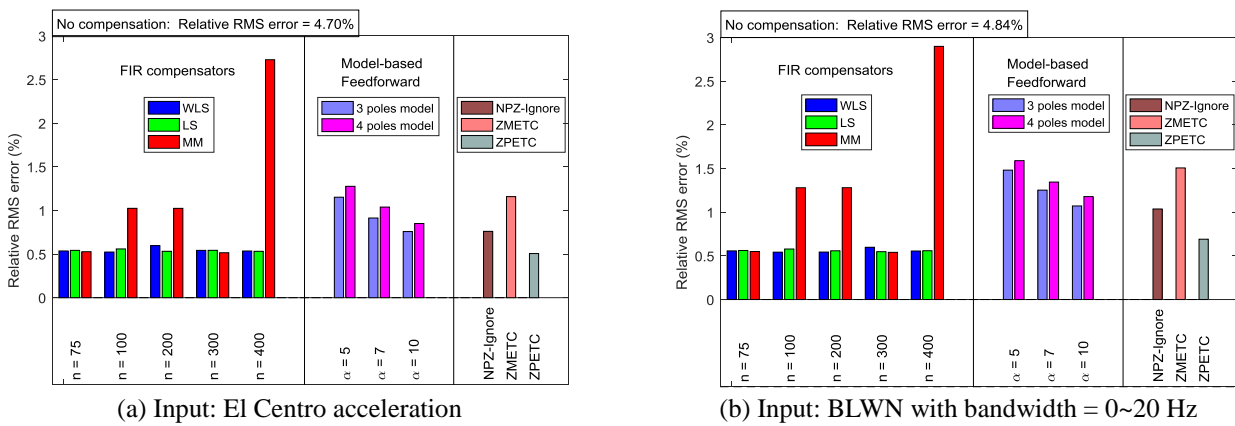


Fig. 11 Relative RMS error between the desired and measured displacement of the actuator

6.2.2 Time delay

The averaged time delay calculated based on Eq. (17) is summarized in Fig. 10. The ‘1 ms’ line is also shown in this figure as the goal of delay compensation. In plot (a), when the frame is subjected to El Centro record, most of the FIR compensators have successfully reduced the time delay from 16.03 ms (RTHS without compensation) to under 1 ms, and in fact, the calculated delays are in small negative values, which indicate phase lead. However, the leading time is very small (less than 1 ms) that the input and output of the servo-hydraulic actuator can still be effectively considered as ‘synchronized’.

Instead of phase leading, another reason that may cause the negative value in the delay calculation is the numerical error in phase calculation. This error occurs because the plant is not fully excited across the frequency domain when the frame is subjected to earthquake inputs. Three out of 5 FIR compensators obtained using MM scheme are showing worse compensation performance than the other FIR compensators. One interesting observation is that ZPETC compensator also has achieved very good delay compensation result. It also can be observed that by increasing the value of α , the time delay associated with the model-based compensators decreases, which is a

property explained in (Carrion and Spencer 2007). Fig. 10(b) shows the delay comparison when the frame is subjected to the BLWN. Comparing to other compensators, all the FIR compensators have achieved satisfactory compensation results by reducing the delay from 16.33 ms (RTHS without compensation) to less than 1 ms, except the 3 compensators obtained using MM scheme.

6.2.3 Relative RMS error between the desired and measured displacement of the actuator

The relative RMS error between the desired displacement and the measured displacement of the actuator (Eq. (18)) were calculated for all performed RTHS tests. Fig. 11(a) and 11(b), show the relative RMS error under El Centro and BLWN excitations, respectively.

Fig. 11(a) shows that except 3 FIR compensators obtained using MM scheme, all other FIR compensators and ZPETC reduced the relative RMS error from 4.70% (RTHS without compensation) to around 0.5%. However, when the excitation was BLWN, the smallest values for relative RMS error were obtained by FIR compensators (except the 3 based on MM scheme) (see Fig. 11(b)).

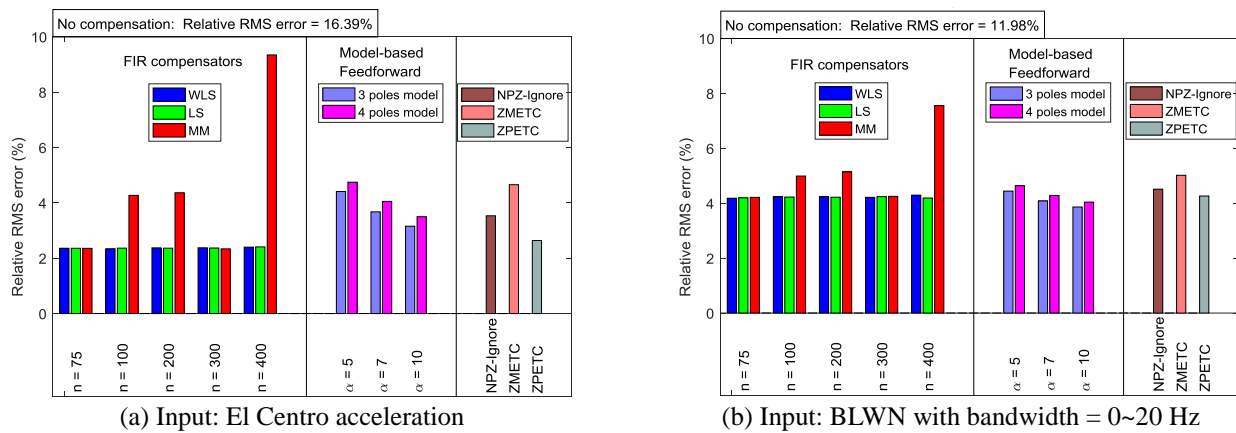


Fig. 12 Relative RMS error between the response of RTHS test and simulated response of the entire frame

6.2.4 Relative RMS error between the response of RTHS test and simulated response of the entire frame

The relative RMS errors (Eq. (19)) obtained from RTHS by using different compensators are all summarized in Fig. 12. Fig. 12(a) shows the relative RMS error when the frame is subjected to El Centro ground motion. The proposed FIR compensators obtained from LS and WLS optimization schemes have successfully reduced the relative RMS error from 16.39% to a low error around 2.35%, which are indicated as the more accurate compensators compared to the others. It also can be seen that the different numbers of parameters in the proposed FIR compensators do not affect the results significantly. However, 3 out of 5 FIR compensators obtained using MM scheme have shown larger errors (more than 4%) which are more than some of the other compensators. The model-based feedforward compensators, NPZ-Ignore, ZMETC and ZPETC compensators all have been able to reduce the relative RMS error under 5%. Fig. 12(b) shows the comparison results when the frame is subjected to the BLWN. It can be observed that most of the compensators performed well and have obtained close results except the 3 FIR compensators obtained using MM scheme.

7. Conclusions

A discrete-time, feedforward compensator using FIR filter formulation is proposed in this paper. The proposed compensator is obtained via different optimization schemes to provide optimal compensation performance for a relatively high frequency bandwidth (0~30 Hz). In addition, by directly developing the compensator in discrete-time domain, the implementation error during the continuous-time to discrete-time conversion is also avoided.

The efficacy and effectiveness of the proposed compensators have been examined in both numerical and experimental compensation studies, and demonstrated in a series of RTHS tests. Meanwhile, the model-based feedforward compensator, NPZ-Ignore, ZMETC and ZPETC compensators have also been implemented and investigated in the studies. The results show that the

proposed FIR compensators can effectively reduce the time delay and relative RMS error between the input and output of the plant system, and demonstrated a better performance than these existing feedforward compensators. Three main observations about the performance of the proposed compensators can be listed as below:

- From the results obtained in section 5, all the proposed compensators can effectively reduce time delay in the presence of different white noises with low (0~10 Hz), medium (0~20 Hz) and high frequency (0~30 Hz) contents.
- From the results obtained in section 5, it is shown that as the number of parameters (n) used in FIR compensator increases and the cut off frequency (f_c) decreases, the compensation performance of the resulting compensator will be improved.
- From the results obtained in section 6, the compensators obtained from WLS and LS schemes leads to better RTHS compensation than those designed by using MM scheme.

The performance of the resulting FIR compensators is sensitive to the accuracy of the identified plant model, as well as the noise level from the laboratory environment. If a significant amount of noise is present in the RTHS loop, the performance may deteriorate the performance of the FIR compensator. Future research will be conducted to improve the robustness of the proposed compensator under varying specimen conditions (e.g., stiffness change) and high levels of disturbances.

References

- Ahmadizadeh, M., Mosqueda, G. and Reinhorn, A.M. (2008), "Compensation of actuator delay and dynamics for real-time hybrid structural simulation", *Earthq. Eng. Struct. D.*, **37**(1), 21-42.
- Åström, K.J., Hagander, P. and Sternby, J. (1984), "Zeros of sampled systems", *Automatica*, **20**(1), 31-38.
- Butterworth, J.A., Pao, L.Y. and Abramovitch, D.Y. (2008), "The effect of nonminimum-phase zero locations on the performance of feedforward model-inverse control techniques in discrete-

- time systems”, *Proceedings of the 2008 American Control Conference*, Westin Seattle Hotel, Seattle, Washington, USA.
- Carrion, J.E. and Spencer, Jr., B.F. (2007), “Model-based strategies for real-time hybrid testing”, NSEL-006, University of Illinois at Urbana-Champaign, Champaign-Urbana, IL, USA.
- Carrion, J.E., Spencer, Jr., B.F. and Phillips, B.M. (2009), “Real-time hybrid simulation for structural control performance assessment”, *Earthq. Eng. Eng. Vib.*, **8**(4), 481-492.
- Chae, Y., Kazemibidokhti, K. and Ricles, J.M. (2013), “Adaptive time series compensator for delay compensation of servo-hydraulic actuator systems for real-time hybrid simulation”, *Earthq. Eng. Struct. D.*, **42**(11), 1697-1715.
- Chen, C. (2007), “Development and numerical simulation of hybrid effective force testing method”, Ph.D. Dissertation, Lehigh University, Bethlehem, PA.
- Chen, C. and Ricles, J.M. (2009a), “Analysis of actuator delay compensation methods for real-time testing”, *Eng. Struct.*, **31**(11), 2643-2655.
- Chen, C. and Ricles, J.M. (2009b), “Improving the inverse compensation method for real-time hybrid simulation through a dual compensation scheme”, *Earthq. Eng. Struct. D.*, **38**(10), 1237-1255.
- Chen, C. and Ricles, J.M. (2010), “Tracking error-based servohydraulic actuator adaptive compensation for real-time hybrid simulation”, *J. Struct. Eng. - ASCE*, **136**(4), 432-440.
- Chonhenchob, V., Singh, S.P., Singh, J.J., Stallings, J. and Grewal, G. (2012), “Measurement and analysis of vehicle vibration for delivering packages in small-sized and medium-sized trucks and automobiles”, *Packaging Technol. Sci.*, **25**(1), 31-38.
- Darby, A.P., Blakeborough, A. and Williams, M.S. (1999), “Real-time substructure tests using hydraulic actuator”, *J. Eng. Mech.*, **125**(10), 1133-1139.
- Darby, A.P., Blakeborough, A. and Williams, M.S. (2001), “Improved control algorithm for real-time substructure testing”, *Earthq. Eng. Struct. D.*, **30**(3), 431-448.
- Darby, A.P., Williams, M.S. and Blakeborough, A. (2002), “Stability and delay compensation for real-time substructure testing”, *J. Eng. Mech.*, **128**(12), 1276-1284.
- Dyke, S.J., Spencer, Jr., B.F. Quast, P. and Sain, M.K. (1995), “Role of control-structure interaction in protective system design”, *J. Eng. Mech.*, **121**(2), 322-338.
- Fu, Y. and Dumont, G.A. (1989), “Choice of sampling to ensure minimum-phase behaviour”, *IEEE T. Autom. Contr.*, **34**(5), 560-563.
- Gao, X., Castaneda, N. and Dyke, S.J. (2013), “Real time hybrid simulation: from dynamic system, motion control to experimental error”, *Earthq. Eng. Struct. D.*, **42**(6), 815-832.
- Gillespie, T.D. and Sayers, M. (1981), “Role of road roughness in vehicle ride”, *Proceedings of the 60th Annual Meeting of the Transportation Research Board*, Washington District of Columbia, United States.
- Gomez, D., Dyke, S.J. and Maghareh, A. (2015), “Enabling role of hybrid simulation across NEES in advancing earthquake engineering”, *Smart Struct. Syst.*, **15**(3), 913-929.
- Goodwin, G.C., Graebe, S.F. and Salgado, M.E. (2001), *Control System Design*, Prentice Hall.
- Gross, E., Tomizuka, M. and Messner, W. (1994), “Cancellation of discrete time unstable zeros by feedforward control”, *J. Dyn. Syst. Meas. Control*, **116**(1), 33-38.
- Hagiwara, T. (1996), “Analytic study on the intrinsic zeros of sampled-data systems”, *IEEE T. Autom. Contr.*, **41**(2), 261-263.
- Horiuchi, T., Nakagawa, M., Sugano, M. and Konno, T. (1996), “DEVELOPMENT OF A REAL-TIME HYBRID EXPERIMENTAL SYSTEM WITH ACTUATOR DELAY COMPENSATION”, *Proceedings of the 11th World Conference on Earthquake Engineering*, Acapulco, Mexico.
- Horiuchi, T., Inoue, M., Konno, T. and Namita, Y. (1999), “Real-time hybrid experimental system with actuator delay compensation and its application to a piping system with energy absorber”, *Earthq. Eng. Struct. D.*, **28**(10), 1121-1141.
- Jung, R.Y. and Shing, P.B. (2006), “Performance evaluation of a real-time pseudodynamic test system”, *Earthq. Eng. Struct. D.*, **35**(7), 789-810.
- Kailath, T., Sayed, A.H. and Hassibi, B. (2000), *Linear Estimation*, Prentice Hall.
- Marlin, T.E. (2000), *Process control: designing processes and control systems for dynamic performance*, McGraw-Hill.
- MATLAB (Version R2014a), The MathWorks, Inc., Natick, Massachusetts, USA.
- Nakashima, M. and Masaoka, N. (1999), “Real-time on-line test for MDOF systems”, *Earthq. Eng. Struct. D.*, **28**(4), 393-420.
- Oppenheim, A.V. and Schaffer, R.W. (2010), *Discrete-time Signal Processing*, Pearson.
- Ou, G., Ozdagli, A.I., Dyke, S.J. and Wu, B. (2015), “Robust integrated actuator control: experimental verification and real-time hybrid-simulation implementation”, *Earthq. Eng. Struct. D.*, **44**(3), 441-460.
- Phillips, B.M. and Spencer, Jr., B.F. (2011), “Model-based feedforward-feedback tracking control for real-time hybrid simulation”, NSEL-028, University of Illinois at Urbana-Champaign, Champaign-Urbana, IL, USA.
- Phillips, B.M. and Spencer, Jr., B.F. (2013), “Model-based feedforward-feedback actuator control for real-time hybrid simulation”, *J. Struct. Eng. - ASCE*, **139**(7), 1205-1214.
- Phillips, B.M., Takada, S., Spencer, Jr., B.F. and Fujino, Y. (2014), “Feedforward actuator controller development using the backward-difference method for real-time hybrid simulation”, *Smart Struct. Syst.*, **14**(6), 1081-1103.
- Schneider, A.M., Kaneshige, J.T. and Groutage, F.D. (1991), “Higher order s-to-z mapping functions and their application in digitizing continuous-time filters”, *Proceedings of the IEEE*, **79**(11), 1661-1674.
- Smith, J.O. (2008), *Introduction to Digital Filters: With Audio Applications*, W3K.
- Tomizuka, M. (1987), “Zero Phase Error Tracking Algorithm for Digital Control”, *J. Dyn. Syst. Meas. Control*, 109.
- Tyan, F. and Tu, S.H. (2015), “A Lyapunov based multi-level controller for semi-active suspension system with an MRF damper”, *Asian J. Control.*, **17**(2), 615-625.
- Wen, J.T. and Potsaid, B. (2004), “An experimental study of a high performance motion control system”, *Proceedings of the American Control Conference*, Boston, MA, USA.

BS